ZeroEcg: Zero-Sensation ECG Monitoring By Exploring RFID MOSFET

Wenli Jiao[12], Ju Wang[123*], Xinzhuo Gao[13], Long Du[13], Yanlin Li[12], Lili Zhao[1], Dingyi Fang[1234], Xiaojiang Chen[1234]
[1]Northwest University, Xi'an, Shaanxi, China
[2]Shaanxi International Joint Research Centre for the Battery-Free Internet of Things; [3]Xi'an Advanced Battery-Free Sensing and Computing Technology International Science and Technology Cooperation Base;
[4]Xi'an Key Laboratory of Advanced Computing and Software Security
{jiaowenli,gaoxinzhuo,dulong,yanlinli2579}@stumail.nwu.edu.cn,{wangju,zhaolili,dyf,xjchen}@nwu.edu.cn

ABSTRACT

ECG monitoring during human activities is crucial since many heart attacks occur when people are exercising, driving a car, operating a machine, etc. Unfortunately, existing ECG monitoring devices fail to timely detect abnormal ECG signals during activities due to the need for many cables or a sustained press on devices (e.g., smartwatches). This paper introduces ZeroEcg, a wireless, battery-free, lightweight, electronic-skin-like tag integrated with commodity RFIDs, which can continuously track a user's ECG during activities. By exploring and leveraging the RFID MOSFET switch, which is traditionally used for backscatter modulation, we map the ECG signal to the RFID RSS and phase measurement. It opens a new RFID sensing approach for sensing any physical world variable that can be translated into voltage signals. We model and analyze the RFID MOSFET-based backscatter modulation principle, providing design guidance for other sensing tasks. Real-world results illustrate the effectiveness of ZeroEcg on ECG sensing.

CCS CONCEPTS

• **Hardware → Wireless devices**; **Sensor devices and platforms**.

*Corresponding author.

ACM MobiCom '24, November 18–22, 2024, Washington D.C., DC, USA

ACM ISBN 979-8-4007-0489-5/24/11
https://doi.org/10.1145/3636534.3690690

KEYWORDS

Wearable ECG sensing, RFID, Backscatter, Internet of Things

ACM Reference Format:
Wenli Jiao[12], Ju Wang[123*], Xinzhuo Gao[13], Long Du[13], Yanlin Li[12],, Lili Zhao[1], Dingyi Fang[1234], Xiaojiang Chen[1234]. 2024. ZeroEcg: Zero-Sensation ECG Monitoring By Exploring RFID MOSFET. In *The 30th Annual International Conference on Mobile Computing and Networking (ACM MobiCom '24), November 18–22, 2024, Washington D.C., DC, USA.* ACM, New York, NY, USA, 15 pages. https://doi.org/10.1145/3636534.3690690

1 INTRODUCTION

An ElectroCardioGram (ECG) [24, 58] wave shows how the heart is functioning since the electrical ECG wave causes the heart muscle to squeeze and pump blood [27]. Tracking the heart's ECG waves during human activities is important since many heart diseases occur when people are active. For example, in North America and Europe, heart attacks during sports range from 500 to 1000 per million per year [3]. For instance, it is reported that a man dies of a heart attack while running on a treadmill at a gym [32], and a man suffers a heart attack while driving and dies in a car [33]. More reports show industrial workers die of heart attacks caused by potential excessive fatigue, e.g., workers in Amazon [7], Nissan [40], Faurecia [9], Cement [23], etc.

Imagining if there is a battery-free, lightweight, and wireless device that can monitor the user's ECG signals *continuously and long-term*, then many lives could be saved since the golden hour for rescuing heart-related diseases is short, usually within 10~60 mins [49, 59]. For example, such a device could continuously monitor ECG signals of patients in a hospital bed, with the wireless receiver installed at the bedside or on the ceiling. Similarly, it could also be used to provide around-the-clock ECG monitoring for discharged or wheelchair-bound patients at home, with the receiver installed under the wheelchair seat. In this way, if anomalies are detected in patients' ECG signals, the device could alert

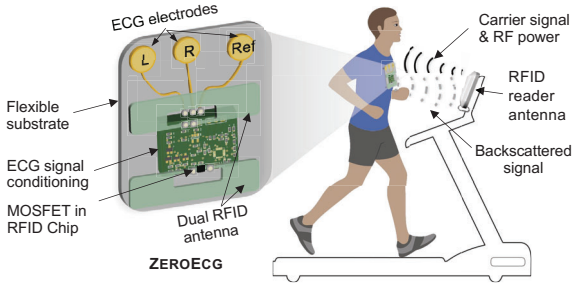

Figure 1: ZEROECG system.

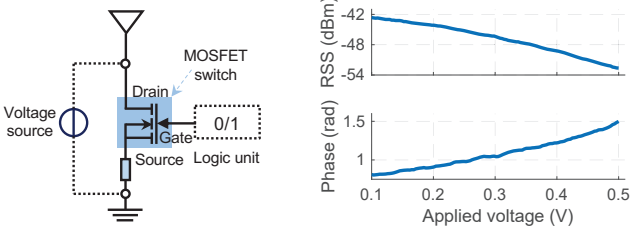

(a) Simplified RFID tag (b) RSS/phase *vs*. Voltage

Figure 2: The RSS/phase of an RFID tag changes with an external voltage applied to the chip.

doctors in time. Furthermore, this device could also be applied in a gym's treadmill, continuously monitoring the ECG signal of users during exercise. The development of such a battery-free and lightweight wireless device holds great potential for long-term ECG monitoring in our daily lives.

Existing ECG devices, however, have difficulty when it comes to long-term and continuous monitoring, particularly during user activities, because they usually require connecting many cables and carrying bulky equipment (e.g., medical ECG machine [22, 26, 34]), or a sustained press on devices with hands (e.g., smart watches [21, 31]). Although existing stick-on, Bluetooth-based ECG devices [15] avoid cable connections and continuous finger pressing, they require frequent charging, impeding long-term ECG tracking.

This paper introduces ZEROECG, a wireless, battery-free, lightweight, electronic-skin-like tag for ECG sensing, as illustrated in Fig. 1. The receiver is a commodity RFID reader that can estimate the user's real-time ECG wave by tracking the ZEROECG tag's RSS and phase sequence. ZEROECG system is built on the RFID technology since 1) RFID tags are battery-free, lightweight, and flexible, and 2) the RFID system has been widely deployed in many scenarios for wireless tracking and managing items/equipment, e.g., modern gyms [11, 28] and industries [14]. Unlike existing RFID-based sensing systems, which either cannot sense electrical signals such as ECG signals[1] [51, 57, 60, 66, 67, 69] or suffer from high-power consumption on data conversion and modulation due to the need for high-power MCU and/or ADC/DAC (e.g., COTS sensory chip [4, 20], WISP [63], and GoodID [52]), hindering long-term sensing, our ZEROECG system can modulate ECG signals on an RFID tag's backscatter signal in an ultra-low-power manner. Our key observation is that RSS and phase measurements of an RFID tag vary with a voltage applied to Drain-Source ports of the tag's MOSFET switch[2], due to changes in the MOSFET impedance caused by the applied voltage, as illustrated in Fig. 2. Thus, by applying an ECG signal obtained from electrodes and conditioned to an RFID tag's MOSFET, we realize a COTS RFID-based ultra-low-power backscatter modulation approach that modulates the ECG signal to the tag's RSS and phase measurements, which is detailed in Section 3.1.

The proposed modulation method has three advantages: (*i*) it eliminates the need for A/D conversion, reducing the power consumption; (*ii*) it eliminates the need for an external logic control unit, simplifying the ECG sensing device greatly; (*iii*) it reuses the RFID tag's backscatter signals for transmitting both the tag's digital ID code and the sensor's analog reading simultaneously, achieving wireless, ultra-low-power and low-cost sensing and communication. These three advantages deliver an opportunity for miniaturized, flexible wearable devices, such as our proposed wireless ECG tracking patch.

There are two challenges when applying the backscatter modulation approach to real-world systems.

Challenge 1: Removing reader's strong interference. As mentioned, we apply the ECG signal to RFID MOSFET for backscatter modulation. The MOSFET is connected to a tag's antenna by default, as illustrated in Fig. 2. Thus, the MOSFET drain-source voltage is a superposition of the reader's signal and the ECG signal. The challenge is that the voltage of ECG signals is extremely weak (e.g., 10 μV~1 mV [61]), compared to the induced voltage on the tag antenna generated by the reader's high-power signal (e.g., around 10 mV~300 mV, depending on the reader-tag distance). As a result, the MOSFET drain-source voltage is dominated by the reader's signal, and one cannot estimate ECG signals correctly.

To deal with this challenge, a naive solution is adding a bypass capacitor to MOSFET in parallel to filter out the reader's strong interference signal. However, it would result in an impedance mismatch between the tag antenna and chip, shortening the working distance to less than half a meter. To remove the interference without reducing the working range significantly, our solution is to jointly quantify electric elements on the impedance matching and the filter performance. By finding a feasible solution that meets all requirements, we estimate ECG signals accurately and

[1]Existing RFID-based passive sensing systems leverage the target-induced changes in a tag's antenna impedance or the signal phase and RSS for sensing. However, electrical ECG signals cannot cause those changes directly.
[2]MOSFET is inside a tag's chip and used for backscatter communication.

extend the working range from 0.3 m to 2 m compared to the naive design. We detail the design in Section 3.2.

Challenge 2: Battery-free ECG signal conditioning. Raw ECG signals collected from electrodes are feeble and prone to be noisy due to other biopotential signals (e.g., the ElectroMyoGraphic signal [55]) or electrode placement offsets caused by body motion. Using an ECG signal conditioning scheme is a common practice to extract, amplify, and filter small ECG signals. However, the operation of amplification and filtering requires consuming power (e.g., 340~400 μW even for a single channel, low-power ECG chip AD8232 [17]). To power such an ECG signal conditioning circuit, one may employ multiple transmitters and beamforming [46, 54]. However, it could increase the system cost. Another solution is using a high-gain antenna for our ZeroEcg tag, so that the tag can harvest enough power. However, a high-gain antenna typically has a large size (e.g., a 5 dBi rubber duck antenna has a length of 38.1 cm [8]), rendering it unsuitable for miniaturized wearable devices. Therefore, the challenge is how to continuously provide sufficient power under the constraint of a small-size and low-gain tag antenna, as well as without increasing the system cost.

To overcome this challenge, we rethink the conventional energy harvesting circuit and analyze the impact of the rectifier stage number on the harvested power. By finding the optimal stage number, we can harvest the maximum power for the ZeroEcg tag even with a small size and low-gain antenna. It enables continuous and battery-free ECG sensing. The design is detailed in Section 3.3.

We build a prototype of ZeroEcg tag by using a flexible printable circuit and a commodity RFID tag. We conduct extensive experiments to evaluate its ECG sensing accuracy with a commodity RFID reader under different scenarios. Results show that: (*i*) ZeroEcg achieves more than 95.8% ECG sensing accuracy on a single user and more than 88.8% accuracy on 10 concurrent users; (*ii*) it is robust to environment noise, user motion, user's clothes, relative position changes between the reader and the tag, and NLoS scenarios; (*iii*) it reduces power consumption by 96.5% and cost by 94.4%, compared with the low-cost commercial Wellue® ECG monitoring device [16].

This paper makes the following **contributions**. By exploring and leveraging the MOSFET electronic characteristics of commodity RFID tags, we discover a new way for battery-free, ultra-low-power, and wireless sensing, and validate it on ECG sensing. We propose a theoretical model to quantify the relationship between the MOSFET drain-source voltage and the RFID RSS/phase, providing guidance for designing RFID-MOSFET-based other sensing systems. To the best of our knowledge, ZeroEcg is the first battery-free, low-cost ECG sensing system that works with commodity RFIDs. Extensive experiments demonstrate the effectiveness of ZeroEcg under varying conditions.

2 BACKGROUND

2.1 RFIDs

Fig. 3 shows an architecture of commodity RFID systems, which include an RFID reader and at least one tag. The RFID tag is cheap and battery-free (i.e., without battery). The reader transmits a high-power carrier signal to power up the tag, and then the tag communicates with the reader by reflecting or non-reflecting the carrier signal. For example, "reflection" means "1-bit" and "non-reflection" means "0-bit", called On-Off Key (OOK) modulation. At the reader side, signal features like RSS and phase, can be estimated from the tag's backscattered signal.

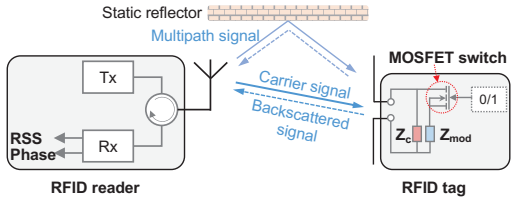

Figure 3: Architecture of RFID systems.

To perform the "reflection" or "non-reflection", commodity RFID tags use a MOSFET switch to connect or not connect a modulation resistor [45], leading to low and high reflection coefficients Γ^L and Γ^H. They are expressed as follows:

$$\begin{aligned} &\text{Non-reflection:} \quad \Gamma^L = \frac{Z_c - Z_a^*}{Z_c + Z_a}, \\ &\text{Reflection:} \quad\quad \Gamma^H = \frac{Z_c || Z_{mod} - Z_a^*}{Z_c || Z_{mod} + Z_a}, \end{aligned} \tag{1}$$

where Z_c is the chip's original impedance, Z_{mod} is the modulation resistor's impedance, and Z_a is the antenna impedance.

According to Nikitin *et al.* [56], a tag's RSS (in dBm) measured by an RFID reader can be modeled as the magnitude difference between the low and high reflection coefficients (i.e., Γ^L and Γ^H) as follows:

$$\text{RSS} = 20 \log_{10} \left(\sqrt{P_{tag}} \cdot |\Gamma^H - \Gamma^L| \right) - P_{loss}, \tag{2}$$

where, P_{tag} is the received power at the tag antenna and P_{loss} is the power attenuation due to the signal propagation. Similarly, the phase (in rad) can be expressed as [56]:

$$\text{Phase} = \arctan \left(\frac{im(\Gamma^H - \Gamma^L)}{re(\Gamma^H - \Gamma^L)} \right) + \phi_0, \tag{3}$$

where ϕ_0 represents the sum of phase responses of the transmitter, receiver, and multipath channel. The P_{tag}, P_{loss}, and ϕ_0 are constant values given a static environment.

2.2 ECG Signals

In general, the ECG signal represents the electrical activity of the heart and is measured as the voltage difference between two points around the heart on the human skin. To obtain ECG signals, a dedicated machine in hospitals uses 10 electrodes and attaches them to 10 points on the limb and chest of a human body [24]. Fig. 4 shows an ECG wave that contains three waves, i.e., P, QRS, and T wave. The most important one is the QRS wave, which represents the depolarization of ventricles. An abnormal QRS indicates a disturbance in the conduction of electrical impulses through the ventricles. In addition, the R-R interval is the reciprocal of the heart rate (i.e., 60/bpm), which is important for diagnosing arrhythmia.

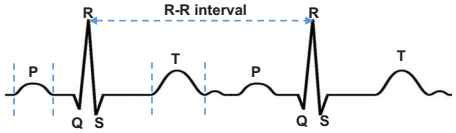

Figure 4: An ECG signal contains P, QRS, and T waves.

3 SYSTEM DESIGN

3.1 Ultra-Low-Power Backscatter Modulation based on RFID MOSFET

3.1.1 The MOSFET Based Modulation Principle. As we explained in Section 2.1, commodity RFID tags use a MOSFET switch for OOK backscatter modulation [29]. Fig. 5 shows a typical structure of N-type MOSFET, which has three ports (i.e., Gate, Source, and Drain) and substrate. Usually, inside the MOSFET, the Source port and the P-substrate are connected. When the Gate is closed, i.e., the Gate-Source voltage $V_{gs} = 0\ V$, the MOSFET can be viewed as a PN junction, as shown in the right of Fig. 5. There is a space charge region between P-type and N-type material regions, forming a reverse built-in electric field [64]. Applying an external electric field V_{sd} would change the electron distribution in the space charge region and weaken the reverse built-in electric field. Hence, the PN junction works like a variable resistance which changes by the applied voltage. Theoretically, the IV curve of the PN junction is modeled as follows [62]:

$$I = I_s \left(e^{\frac{qV_{sd}}{nkT}} - 1 \right), \tag{4}$$

where V_{sd} is the the source-drain voltage, I_s is saturation current, k is Boltzmann's constant $1.38 \times 10^{-23} J/K$, q is the electron charge $1.6 \times 10^{-19} C$, n is the ideality factor, and T is the temperature. Therefore, the equivalent resistance of the PN junction is modeled as follows:

$$R_{mos} = \frac{nkT}{qI_s} e^{-\frac{qV_{sd}}{nkT}} = f(V_{sd}). \tag{5}$$

The parameters I_s, k, q, n, T are fixed for a room temperature. Thus, we have $R_{mos} \propto V_{sd}$, which is the basis of using MOSFET for modulation, i.e., *the Source-Drain voltage V_{sd} can change the equivalent impedance R_{mos} of MOSFET, which will result in changes in the RFID phase and RSS.*

So, how can we apply a voltage to the source-drain ports of an RFID MOSFET which usually is inside a tag's chip? In this paper, through experimental results, we show that applying a voltage to an RFID chip is equivalent to applying the voltage across the MOSFET's source-drain ports. Specifically, we compare the IV curves of an RFID tag's chip and a COTS MOSFET device (i.e., NTK3134N). The experimental setup is shown in Fig. 6(a) where we apply a voltage source to the RFID chip or the MOSFET source-drain ports, and then measure the source voltage U_1 and RFID chip/MOSFET voltage U_2. The resistor R_0 has a fixed value. The current in this circuit is calculated as $(U_1 - U_2)/R_0$. The two measured IV curves are shown in Fig. 6(b) and Fig. 6(c). As we can see, patterns of IV curve variations for the RFID chip and the COTS MOSFET are nearly identical, except for a slight difference in current due to the fabrication difference of the RFID chip and MOSFET. It implies that applying the voltage to the RFID chip is equivalent to applying the voltage to the MOSFET's source-drain ports.

Fig. 6(b) also shows that the IV curve of an RFID chip is nonlinear, indicating the equivalent resistance of the RFID chip is not constant but varies with the applied voltage, which verifies the basis of using RFID MOSFET for backscatter modulation shown in Eqn. (5).

3.1.2 Model the Relationship between V_{sd} and RSS/Phase. Recall that a MOSFET switch is connected in series with the modulation resistor as illustrated in Fig. 3. In backscattering, the logic unit in the RFID chip controls the MOSFET's Gate-Source voltage V_{gs} to switch between 0 and V_{work} [3].

- When the V_{gs} is 0, the MOSFET is open and the equivalent resistance is very large and changes with Source-Drain voltage as illustrated in the sub-figure in Fig. 6(c).
- When the V_{gs} is V_{work}, the MOSFET is conducting and the equivalent resistance is small and constant (usually < 2 Ω).

Therefore, the equivalent impedance of the tag's chip can be written as follows:

$$\begin{aligned} V_{gs} = 0: \quad & Z_c^L = Z_c || \left(Z_{mod} + R_{mos} \right), \\ & = Z_c || \left(Z_{mod} + f(V_{sd}) \right), \\ V_{gs} = V_{work}: \quad & Z_c^H = Z_c || Z_{mod} \end{aligned} \tag{6}$$

where Z_c is the chip impedance, Z_{mod} is the impedance of the modulation resistor, and R_{mos} is the equivalent resistance of MOSFET which is a function of V_{sd}. Accordingly, we can

[3]The working voltage of an RFID chip is a constant, usually more than the threshold voltage of MOSFET.

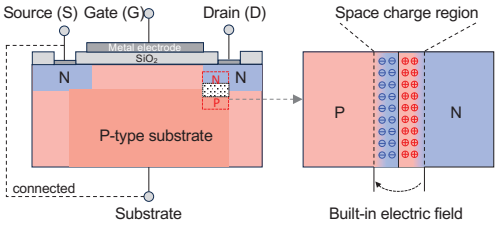

Figure 5: Illustration of MOSFET and the inner PN junction.

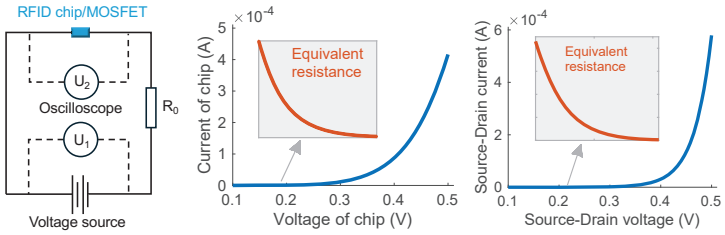

(a) Setup (b) Measured IV of RFID chip (c) Measured IV of MOSFET

Figure 6: IV curve measurement.

rewrite two reflection coefficients Γ^L and Γ^H as:

$$\begin{aligned} \text{Low}: \quad \Gamma^L &= \frac{Z_c^L - Z_a^*}{Z_c^L + Z_a} = \frac{Z_c||(Z_{mod}+f(V_{sd}))-Z_a^*}{Z_c||(Z_{mod}+f(V_{sd}))+Z_a}, \\ \text{High}: \quad \Gamma^H &= \frac{Z_c^H - Z_a^*}{Z_c^H + Z_a} = \frac{Z_c||Z_{mod}-Z_a^*}{Z_c||Z_{mod}+Z_a}, \end{aligned} \tag{7}$$

where Z_a is the impedance of a tag's antenna and Z_a^* is the complex conjugate of Z_a. Then, the reflection coefficient variation $\Delta\Gamma = \Gamma^H - \Gamma^L$ can be expressed as a function of V_{sd}, termed as $\Delta\Gamma = g(V_{sd})$ for simplicity.

By substituting Eqn. (7) into Eqn. (2) and (3), RSS and phase can be written as:

$$\text{RSS} = 20\log_{10}\left(\sqrt{P_{tag}} \cdot |g(V_{sd})|\right) - P_{loss}, \tag{8}$$

$$\text{Phase} = \arctan\left(\frac{im\left(g(V_{sd})\right)}{re\left(g(V_{sd})\right)}\right) + \phi_0, \tag{9}$$

where,

$$g(V_{sd}) = \frac{Z_c||Z_{mod} - Z_a^*}{Z_c||Z_{mod} + Z_a} - \frac{Z_c||\left(Z_{mod} + f(V_{sd})\right) - Z_a^*}{Z_c||\left(Z_{mod} + f(V_{sd})\right) + Z_a}, \tag{10}$$

where Z_c, Z_{mod}, and Z_a are fixed for a given RFID tag.

In summary, the two equations (8) and (9) prove that an RFID tag's RSS and phase measurements will change with an externally applied voltage V_{sd}, providing a general low-power and low-cost backscatter modulation approach by reusing COTS RFID tags.

Verification of the above model. We conduct real-world experiments to verify the model relationship between V_{ds} and a commodity RFID tag's RSS and phase, i.e., Eqn. (8) and (9). Specifically, we apply a sawtooth wave, which has a frequency of 1 Hz, a voltage of 0.1 V~0.5 V, and a current of 1 mA, to the two ports of an LAXCEN N40 tag with NXP G2iL chip [13], as illustrated in Fig. 7(a). Then, we compare the measured RSS and phase values and the simulated RSS and phase values from Eqn. (8) and (9). Note that, (i) we cut off the tag's loop antenna close to the chip to avoid short-circuiting the sawtooth wave; (ii) we use a relatively large current for the sawtooth wave to resist the RFID reader's high power interference signal. We will detail the interference suppression design in the next Section.

Fig. 7(b) shows the measured and simulated phase/RSS values over the sawtooth wave, demonstrating that (i) the

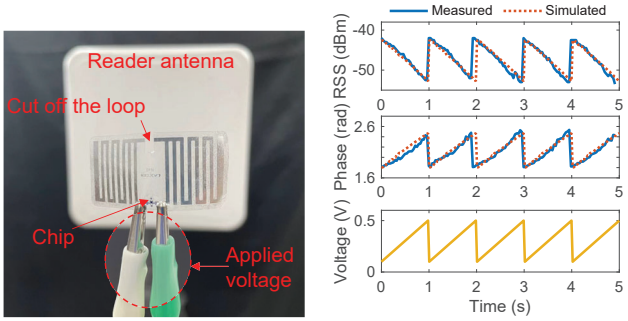

(a) Experimental setup (b) Measurement *vs.* Simulation

Figure 7: Verification of the relationship between the applied voltage and RSS&phase feature.

measured values match the simulated values well, which verifies the model equations Eqn. (8) and (9); (ii) there is a clear and straightforward mapping relationship between the applied voltage and the RSS and phase readings.

3.2 Interference Suppression for Long-Range Backscatter

According to the MOSFET-based modulation principle explained before, we now try to apply ECG signals obtained by electrodes to the RFID MOSFET for ECG sensing. However, the voltage of ECG signals is extremely low (e.g., 10 μV~1 mV [61]), compared to the induced voltage on the tag antenna generated by the reader's high-power signal (e.g., around 10 mV~300 mV depending on the reader-tag distance). Thus, the voltage applied to the RFID tag is dominated by the reader's signal, preventing accurate ECG estimation.

To illustrate the impact of the reader's signal on the ECG sensing, we conduct a benchmark experiment with a commodity RFID reader (i.e., Impinj R420) and a tag (i.e., LAXCEN N40). Following our MOSFET-based modulation approach, we apply the ECG signal sensed by electrodes to two ports of an RFID tag. Fig. 8 (a) and (b) show the measured phase and RSS sequences.[4] The phase and RSS measurements are

[4]To facilitate comparison, we normalize the phase, RSS and ECG signals. Medical applications focus on the pattern of the ECG wave, such as how long the wave lasts, so normalization does not affect the final result.

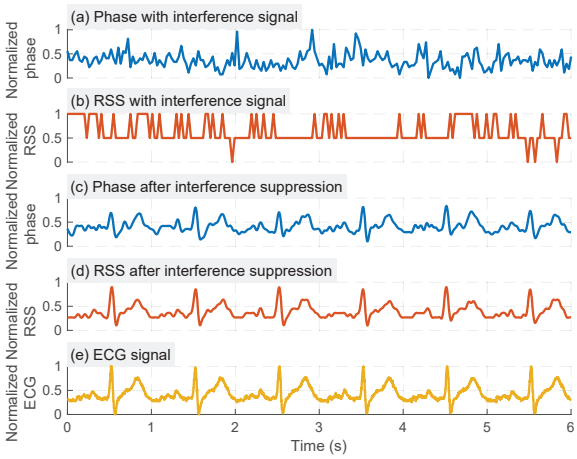

Figure 8: Real-world measured ECG signal *vs.* RSS and phase measurements of an RFID tag. The interfered phase and RSS are shown in (a) and (b). The phase and RSS after interference suppression are shown in (c) and (d). The ECG signal is shown in (e).

very noisy and do not follow the pattern/curve of the applied ECG signal. As a result, one cannot extract the correct ECG signal from the RSS and phase measurements directly.

Understand Interference Signals. To determine the interference signal's root cause, we measure the applied ECG signal at the RFID tag's two ports using an oscilloscope (Tektronix 1000C) in case the reader is off and on. Results are shown in Fig. 9 (a). Obviously, when the reader is off, there is a clear ECG signal (the blue one). When the reader is on, the measured ECG signal becomes a superposition of the original ECG signal and an unknown interference signal (the yellow one). Interestingly, subtracting the clear ECG signal from the interfered one will obtain a periodic square wave signal, as shown in Fig. 9 (b).

In fact, the interference signal comes from the reader which usually sends a continuous wave and a PIE Query command in turn to power up and query a tag [2]. Fig. 10 shows a USRP N210 captured reader's signal when the reader queries an RFID tag, where the signal with high amplitude is the Query signal, while the signal with low amplitude is the continuous wave. When the reader switches between these two signals, the envelope forms a square wave-like signal with a period of 52.8 ms, where the duration of the Query signal is 20.8 ms and the continuous wave is 32 ms. On the other hand, if we look at the zoomed-in interference signal shown in Fig. 9 (c), we find that the interference signal also has a period of 52.8 ms (i.e., $f_{Interference}$=18.9 Hz), where its low-level lasts for 20.8 ms and the high-level lasts for 32 ms. Therefore, the interference signal shown in Fig. 9 (c) is consistent with the reader's signal shown in Fig. 10, validating that the reader's signal interferes with the ECG signal at the RFID tag's antenna.

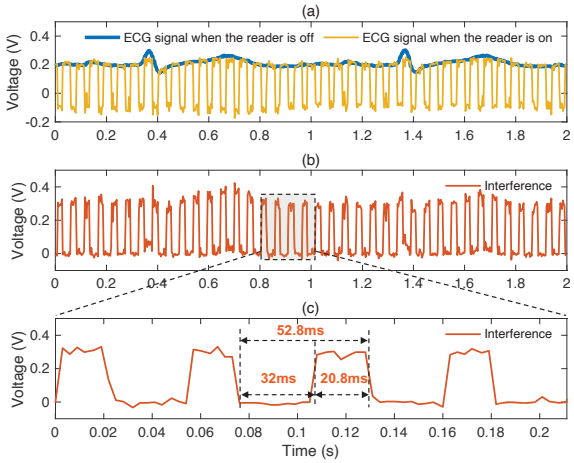

Figure 9: The interfered ECG signal at the tag antenna.

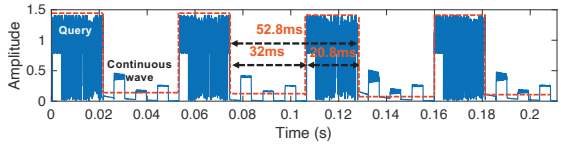

Figure 10: An RFID reader transmits continuous wave and Query command in turn, to power and query tags.

Interference Suppression Design. Our goal is to dampen the interference signal so that one can estimate ECG signals correctly from RSS and phase. Based on the above analysis, a naive solution is to use a bypass capacitor in parallel with the tag due to the frequency difference between the interference signal and the ECG signal. However, adding a bypass capacitor would lead to an impedance mismatch between the tag's antenna and chip, reducing the tag-to-reader distance to no more than half a meter. Because, the signal impinging on the RFID tag is rebounded, and hence the tag cannot harvest sufficient energy to power up itself. *So, the challenge is how to realize impedance matching and interference removal simultaneously.* To this end, we utilize two models to determine the proper interference removal circuit structure and calculate the feasible values of the circuit parameters.

(i) Impedance Matching Model. For an RFID tag, its chip and antenna have complex impedance, i.e., $R + jX$. The antenna impedance is termed as $R_a + jX_a$ and the chip impedance is termed as $R_c + jX_c$. Denote the impedance of the interference suppression circuit as Z_{sup}. The reflection coefficient can be written as follows:

$$\Gamma' = \frac{R_c + jX_c - [(R_a + jX_a)||Z_{sup}]^*}{R_c + jX_c + [(R_a + jX_a)||Z_{sup}]} \tag{11}$$

where Γ' is the reflection coefficient. Let's consider the boundary cases of two impedance matching scenarios:

$$\begin{aligned} &\text{Perfect Matching:} && \Gamma' = 0(-\infty\ dB) && \rightarrow \lim_{Z_{sup}\to\infty} \Gamma' \\ &\text{Severe Mismatching:} && \Gamma' = 1\ (0\ dB) && \rightarrow \lim_{Z_{sup}\to 0} \Gamma' \end{aligned} \tag{12}$$

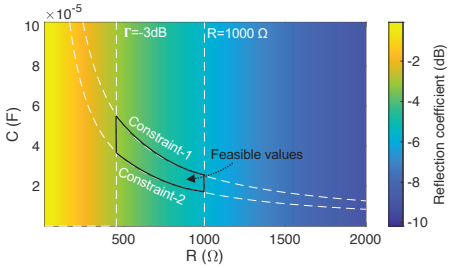

Figure 11: Feasible R, C values.

Therefore, to reach impedance matching, the impedance of Z_{sup} should be as large as possible. Our solution is to add a resistor element in series with the bypass capacitor to increase the impedance Z_{sup}, since 1) the resistor can adjust the new impedance of the paralleled antenna and interference suppression circuit to realize impedance matching and 2) a resistor and a capacitor form an RC filter, absorbing the interference signal. To satisfy a basic impedance matching, the reflection coefficient usually should be below -3 dB.

(ii) Filter model. The foregoing model indicates that the interference suppression circuit contains a capacitor and a resistor, i.e., an RC filter. The RC filter absorbs the interference signal. To calculate optimal RC values, we consider two key parameters of the RC filter:

- Damping Coefficient ζ, which reflects the performance of the interference suppression and can be written as:

$$\zeta = \pi RC \cdot f_{Interference}, \tag{13}$$

  where, $f_{Interference}$ is the frequency of the interference signal. To suppress interference signals, the RC filter circuit should be overdamped (i.e., $\zeta > 1$), which means that the RC filter circuit should absorb most of the interference signal energy (about 90%). Then, we have the first constraint for RC values:

$$\text{Constraint 1: } \pi RC \cdot f_{Interference} > 1. \tag{14}$$

- Cutoff Frequency f_{cutoff}, which allows the passage of interference signals while blocking ECG signals. The cutoff frequency of an RC filter can be written as:

$$f_{cutoff} = \frac{1}{2\pi RC}, \tag{15}$$

$$f_{ECG} < f_{cutoff} < f_{Interference}, \tag{16}$$

  where, f_{ECG} = 0.5~5 Hz, corresponding to 30~300 bpm. Thus, we have the second constraint:

$$\text{Constraint 2: } 5 < \frac{1}{2\pi RC} < 18.9. \tag{17}$$

Besides, when determining the resistor value, it is crucial to consider the impact of parasitic capacitance. The presence of an internal parasitic capacitor in parallel with the resistor leads to a significant reduction in total impedance as frequency increases. Resistors with larger nominal values exhibit higher parasitic capacitance [6]. For instance, even for high-frequency chip resistors, a 1 KΩ resistor experiences impedance drop at frequencies in the hundreds of MHz range due to parasitic capacitance [5]. Thus, we limit the resistor's nominal value to be lower than 1 KΩ.

Finally, considering all constraints from the impedance matching model (i.e., Γ<-3 dB), the filter model (i.e., Eqn. (14) and Eqn. (17)) and the resistor's high-frequency characteristic (i.e., $R \leq 1000\ \Omega$), we can obtain a range of RC feasible solutions, which is the intersection shown in Fig. 11.

Verification of Interference Suppression. Fig. 8 (c) and (d) show the received phase and RSS sequence after the interference suppression. It is clear that phase and RSS show the same pattern as the applied ECG signal, validating the effectiveness of the designed interference suppression circuit.

3.3 Battery-Free ECG Signal Conditioning

Besides the reader's interference signal, there are other interferences in ECG sensing, including the EMG signal and the electrode drift due to body motion. Thus, we need ECG signal conditioning before applying ECG signals to the RFID MOSFET. To this end, we first describe our ECG conditioning front end. Then, we introduce an optimized RF energy harvester design to power up the ECG conditioning front-end continuously, given the constraint of the small-size and low-gain tag antenna.

3.3.1 ECG Conditioning Front-end. The ECG conditioning front-end performs ECG amplification and noise removal. To extract and amplify small ECG signals and filter out unwanted noisy biopotential signals, ZeroEcg employs a COTS ECG conditioning chip AD8232 [17], due to its reliability and ultra-low power consumption (170 μA in operation mode).

As shown in Fig. 6(b), the effective voltage range for backscatter modulation is 100 mV~500 mV. Therefore, the output voltage range of ECG signals should be scaled in this range. To amplify the raw ECG signal from electrodes, the instrument amplifier inside the ECG chip provides an amplification gain of 100× and a common mode rejection ratio (CMRR) of 80 dB. Moreover, we set a second-stage amplification to make sure the output ECG signal is within 100 mV~500 mV.

3.3.2 Battery-free Design. The ECG conditioning circuit (e.g., amplification and filtering) usually consumes power. Even a single channel ultra-low-power ECG chip consumes 340~400 μW as introduced before. Thus, a well-designed energy harvester module is required to achieve continuous battery-free ECG sensing under the constraint of a small-size, low-gain tag antenna (<2 dBi), as well as without increasing the system cost.

In theory, the harvested power of tag can be expressed as $P_{tag} = P_0 \cdot A_{size} \cdot PCE$, where P_0 is the power density per unit

area which is reversely related to the distance. The parameter A_{size} is the antenna size that determines the antenna gain. Therefore, for a small-size antenna with low gain, the rectifier's power conversion efficiency PCE should be maximized to improve the working range.

To overcome this challenge, we rethink the conventional energy harvesting circuit design. The Dickson rectifier has been commonly used in various RF energy harvesting-based IoT tags [42, 47, 53, 63] since it can rectify ultra low input voltage and also has a compact size that is suitable for RF energy harvesting based low-cost battery-free ECG sensing tags. The structure of the rectifier a cascaded stage of capacitors and diodes, as shown in Fig. 13 (a).

In theory, a higher rectifier stage will output higher voltage U. However, it is at the expense of decreased current I in reality due to the power loss on imperfect diodes. Therefore, the traditional solution, i.e., using a high rectifier stage, may not provide the maximum power since $P = UI$. Thus, we need to find the optimal stage number to maximize the harvested power. The harvested power is related to four parameters of the multi-stage rectifier, including (i) the input voltage V_{in}, (ii) the number of stages N, (iii) the voltage drop caused by diodes V_{drp}, and (iv) the load current consumption I_{load}.

Mathematically, the harvested power can be modeled as follows [42]:

$$P_{out} = \frac{\left(N \cdot V_{in} \cdot \alpha - N^2 \cdot \beta - N \cdot V_{drp} - N \cdot I_{load} \cdot \gamma\right)^2}{R_{load}}, \quad (18)$$

where α is related to the impedance match of the antenna and rectifier, β is related to conduction loss due to the load current drawn, and γ is related to the voltage variation due to the changes in the output impedance. The parameters α, β, γ, V_{drp} and I_{load} are fixed for given circuit elements. Therefore, the only way to maximize the harvested power is to optimize the stage number N.

Next, we find the optimal N that maximizes the harvested power P_{out} using numerical analysis based on Eqn. (18). Fig. 12(a) shows the calculated P_{out} over different stage number N and input voltage V_{in}, where the contour line indicates the required power of our ZeroECG tag (i.e., 490 μW). In real-world applications, we also want a long working range between the tag and the reader. A long reader-tag distance corresponds to a low input voltage V_{in} due to the propagation power loss in the air. As we can see, the minimum input voltage V_{in} that can meet the required power of our ZeroECG tag is 430 mV, corresponding to a stage number $N = 6$. That is to say, in order to harvest the maximum power as well as achieve the longest working range, the optimal rectifier stage number in our design is 6.

Verification of our 6-stage rectifier for energy harvesting. We make three Dickson rectifiers with 4-stage, 6-stage, and 8-stage. For each rectifier, we measure the output power at different distances, corresponding to different input voltages. The real-world experimental results in Fig. 12(b) show that the 6-stage rectifier achieves a longer distance than the 4-stage and 8-stage, which verifies our rectifier design.

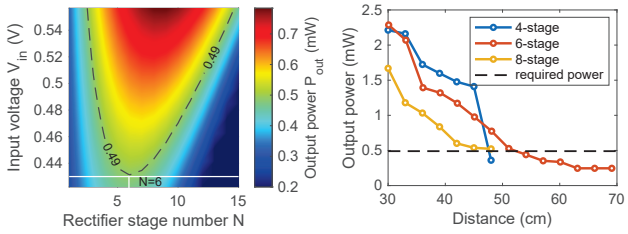

(a) Numerical analysis (b) Experiment verification

Figure 12: Finding the optimal rectifier stage number.

3.4 ECG Estimation

As demonstrated in Fig. 8 (c), (d), and (e), the pattern of RSS and phase sequences after interference suppression is similar/close to the ECG signal. Ideally, one can use either RSS or phase measurement to obtain the ECG signal. However, in real-world applications, surrounding objects such as walls, furniture, etc., will create multipath signals between our ZeroECG tag and the reader, which may break the ECG signal modulated RSS/phase sequence pattern. Moreover, a user's movement/activity would also cause additional RSS/phase variations that are not related to the ECG signal.

To deal with the multipath and user movement, we employ a reference tag and deploy it close to our ZeroECG tag. The reference tag solution has been proven to be effective in removing multipath signals and signal variations due to the sensing tag movement in existing RFID-based sensing systems [51, 66–68]. The high-level idea is that the closely co-located reference tag and sensing tag will suffer from almost the same signal variations or noise due to the static multipath reflection and the user's movement. Thus, a differential RSS/phase measurement between two closely located tags can remove most unwanted signal variations and noise.

After calculating the differential value, we conduct a three-step operation on the differential trace, i.e., interpolating, normalizing, and baseline drift removal, to estimate an accurate ECG signal. The interpolation operation is used to improve the resolution of the recovered ECG waveform since the reading rate is low (around 30 samples per second based on empirical tests). Then, we normalize the RSS/phase trace in a range of 0–1. Finally, we remove the baseline drift by fitting the baseline trend of the raw ECG signal and subtracting the fitted baseline drift line from the raw ECG signal.

4 IMPLEMENTATION

ZeroEcg Tag. Fig. 13(a) shows the overall circuit diagram of ZeroEcg tag, which consists of (i) a backscatter modulation module based on a COTS LAXCEN N40 RFID tag's MOSFET and a passive RC circuit module for interference suppression and impedance matching ($R = 510\ \Omega$ and $C = 47\ \mu$F), (ii) an ECG signal conditioning module, including a COTS AD8232 chip [17] and an ECG scaling circuit, and (iii) an energy harvester with a small size antenna (a gain of 0 dBi) and a 6-stage rectifier.

We choose the LAXCEN N40 RFID tag for two reasons: (i) a relatively small size for the lightweight design, and (ii) it achieves a better modulation performance than other commonly used RFID tags (e.g., ALN-9662 tag [18] and ALN-9740 tag [19]). The rectifier has six Schottky diodes HSMS-285C with a turn-on voltage of 150 mV [30], six 10 pF capacitors, and a 100 μF capacitor at the last stage. The LDO chip TPS7A0220PDBVR [37] outputs a constant supply voltage of 2 V to power the ECG conditioning circuit, which requires a minimum input voltage of 2.4 V. The fabricated ZeroEcg tag prototype is shown in Fig. 13(b). We employ Ecoflex polymer [25] to encapsulate the entire tag to isolate it from the human body as shown in Fig. 13(c).

ECG Electrode. We fabricate the ECG electrode with low-cost copper film and off-the-shelf hydrogels, as shown in Fig. 13 (a). Specifically, the copper is etched by laser engraving technology. Then, the sculpted circular copper foils are pasted on the hydrogel. The end of the copper foil wire is connected to the FPCB circuit through pins to realize the pluggability of the electrodes. Note that, the current hardware prototype only measures the lead-V5 ECG wave. One can implement all chest-lead waves (V1-V6) by integrating multiple electrodes, the multi-channel ECG conditioning chip, and multiple RFID tags.

Reader. We use a commodity RFID reader with only one antenna, i.e., the Impinj RFID reader [1] and an S9028PCL circularly polarized panel antenna with a gain of 9 dBi [10]. The reader is connected to a laptop with an Ethernet cable for RSS and phase readings collection.

5 PERFORMANCE EVALUATION

5.1 Performance Metric and Ground Truth

Metrics. We use three metrics to evaluate ZeroEcg:

- *Correlation Coefficient*, which shows the overall similarity or correlation between the estimated ECG signal X and the ground truth ECG signal Y. Suppose there are n samples, then the correlation coefficient is defined as follows:

$$\text{Coeff} = \frac{\sum_{i=1}^{n}(X_i - \bar{X})(Y_i - \bar{Y})}{\sqrt{\sum_{i=1}^{n}(X_i - \bar{X})^2}\sqrt{\sum_{i=1}^{n}(Y_i - \bar{Y})^2}}. \quad (19)$$

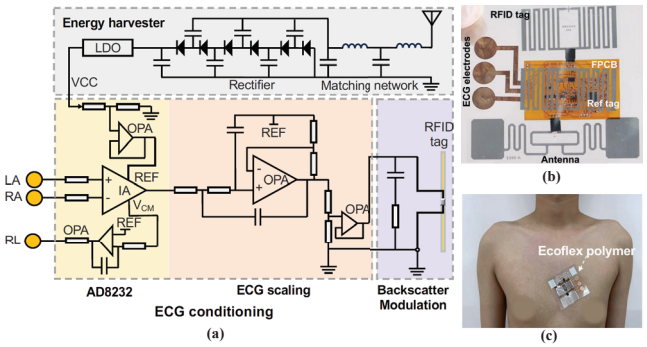

Figure 13: The fabricated ZeroEcg tag.

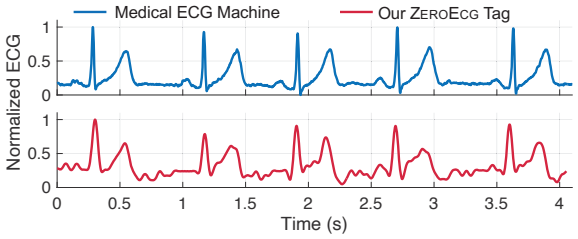

Figure 14: The lead-I ECG wave comparison.

- *QRS Detection Accuracy*, which is the ratio of two QRS wave numbers detected from our estimated ECG (Num_QRS_Est) and the ground truth (Num_QRS_Truth):

$$\text{Accuracy} = \frac{Num\_QRS\_Est}{Num\_QRS\_Truth} \times 100\%. \quad (20)$$

  QRS detection is important for detecting many diseases, such as coronary artery disease, bundle branch block, and cardiac hypertrophy [36, 50].
- *R-R Interval Error*, which is the absolute difference between two R-R intervals calculated from our estimated ECG and the ground truth ECG. Note that the heart rate is the reciprocal of the R-R interval, which is an important indicator for diagnosing arrhythmia.

Ground truth. We collect the ground truth ECG signal via a commodity ECG device Heal Force PC-80B [12]. We use the limb leads with three electrodes, i.e., the left, right, and reference electrodes, which are shown in Fig. 23 (d)-(f).

5.2 Overall ECG Sensing Performance

Comparison with medical ECG machine. To understand the performance of ZeroEcg, we first compare the ECG wave captured by the medical ECG machine and our ZeroEcg system. In this experiment, we use a 12-lead ECG machine (FUKUDA CardiMax FCP-8100) that is used for clinical testing in hospitals. The volunteer is asked to lie on the bed, and attached with 10 electrodes. To test the ECG signal simultaneously, we attach the electrode of our ZeroEcg tag at the same positions as the medical ECG machine, i.e., three electrodes on the user's left wrist, right wrist, and right ankle

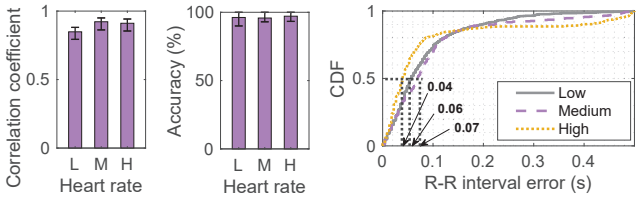

(a) Correlation (b) Accuracy (c) R-R interval error

Figure 15: The overall ECG sensing performance of ZeroECG at three heart rate levels.

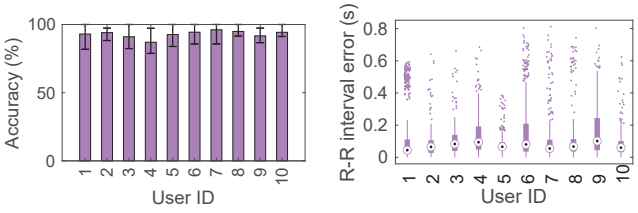

(a) QRS wave detection accuracy (b) R-R interval estimation error

Figure 16: ECG sensing across different users.

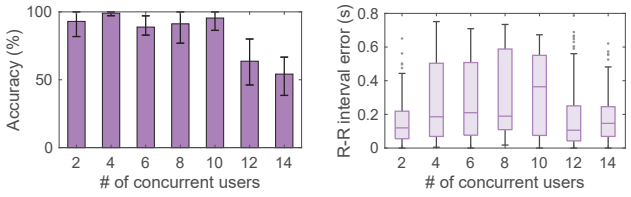

(a) QRS wave detection accuracy (b) R-R interval estimation error

Figure 17: ECG sensing of concurrent users.

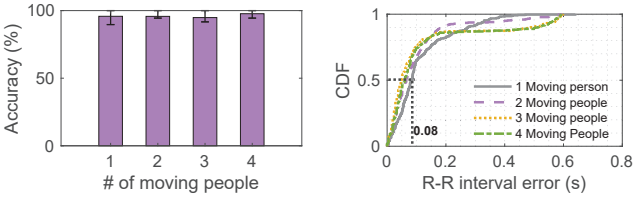

(a) QRS wave detection accuracy (b) R-R interval estimation error

Figure 18: ECG sensing under environmental noise.

respectively. We compare the lead-I ECG wave as shown in Fig. 14. We can see that the measured ECG wave by the medical ECG machine is stable and smooth, and our ECG wave has some noise. Despite that, the pattern of the two waves is close to each other. Their cross-correlation coefficient is 0.9, demonstrating that the ECG sensing accuracy is comparable to a medical ECG machine.

Performance at different heart rate ranges. We estimate ECG signals when a user's heart rate is low (60∼80 bpm), medium (85∼105 bpm), and high (110∼130 bpm), corresponding to daily activities of sitting, walking, and running. In each experiment, we measure 15 traces of ECG signals and each trace lasts for 30 s.[5] The distance between the reader antenna and the ZeroECG tag is 1.2 m. Results are shown in Fig. 15(a). The similarities (or correlations) over 3 heart rate levels are higher than 0.83. Fig. 15(b) shows the QRS detection accuracy over three heart rate levels, which is higher than 95.8%. Fig. 15(c) shows the R-R interval estimation error, where the median errors of three heart rate levels are small, only 0.06 s, 0.07 s, and 0.04 s. The above results imply that ZeroECG can estimate ECG signals accurately.

Performance across different users. Different users have different ECG voltage ranges, which may affect the sensing accuracy. Thus, we evaluate ZeroECG across different users, i.e., 10 users consisting of 5 males (#1–#5), and 5 females (#6–#10). The 10 participants are between 20 and 30 years of age, with a body mass index (BMI) falling within the healthy weight range 18.5∼24.9. None of the participants had reported known pre-existing cardiovascular conditions. [6] The experimental setup is the same as before. Results in Fig. 16 show that the QRS detection accuracy across 10 users is > 87%, and the median R-R interval error is < 0.06 s. It demonstrates the high ECG sensing accuracy of ZeroECG across different users.

Table 1: Comparison with existing ECG devices.

ECG devices	Cost (USD)	Power	Accuracy
Medical machine [26]	600∼1000 [1]	60 W	100%
Portable device [16]	90 [1]	13.875 mW	100%
The work [43]	87 [2]	1.23 mW	–
ZeroECG tag	5 [2]	482.5 μW	95.8%

[1] One-third of the device's market price for a fair comparison.
[2] The summation of the market price of all components and the circuit fabrication cost.

Comparison about power consumption, cost, and accuracy. Table. 1 lists the device cost, power consumption, and sensing accuracy of four ECG sensing devices. The power consumption of our ZeroECG tag is measured via an oscilloscope and ammeter. The power consumption of commercial ECG devices is found in their device specifications. The average power consumption of the ZeroECG tag is 482.5 μW, primarily contributed by the ECG chip AD8232. Compared to a low-cost commercial portable ECG device [16], our ZeroECG tag reduces the power by 96.5% and decreases the device cost by 94.4%. Also, the sensing accuracy of ZeroECG is 95.8%, lower than commercial ECG devices.

[5] Note that we measure each ECG trace with a duration of 30 s because the ground-truth device can only store the ECG signal with a fixed time length.

[6] We recruited ten participants from our lab who volunteered to take part in the experiment. There are no conflicts of interest between the authors and participants. This research protocol has been approved by our IRB.

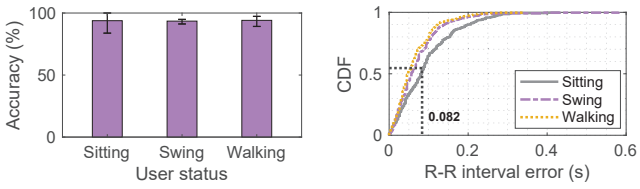

(a) QRS wave detection accuracy (b) R-R interval estimation error

Figure 19: ECG sensing under user motion status.

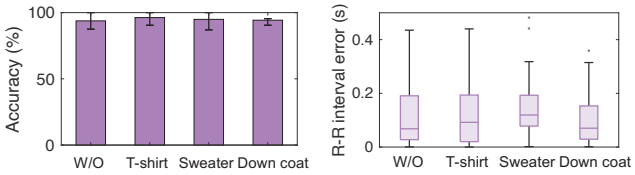

(a) QRS wave detection accuracy (b) R-R interval estimation error

Figure 20: ECG sensing under different clothes.

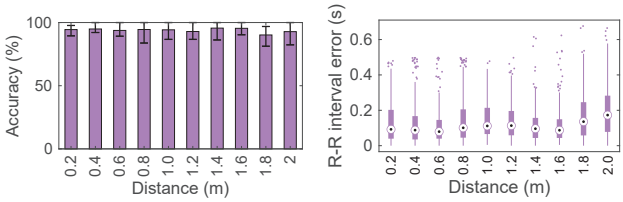

(a) QRS detection accuracy (b) R-R interval estimation error

Figure 21: ECG sensing at different distances.

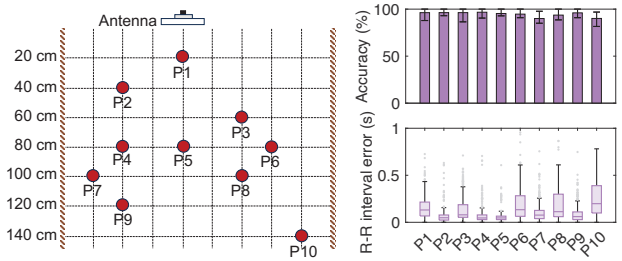

(a) Test locations (b) ECG sensing results

Figure 22: ECG sensing at different relative positions.

5.3 ECG Sensing of Concurrent Users

ZeroEcg can support multiple users simultaneously since a commodity RFID reader can read a maximum of 1100 tags per second [2]. Thus, we evaluate the ECG sensing performance of ZeroEcg on multiple concurrent users. Due to the limited number of fabricated ZeroEcg tags, we evaluate the sensing accuracy when there are 2, 4, 6, 8, 10, 12, and 14 concurrent users. From Fig. 17, we observe that the QRS detection accuracy remains relatively stable and consistently above 88.8% when the number of concurrent tags is 10 or fewer. When the number of concurrent tags is 12 and 14, the accuracy is decreased to 63.6% and 54.1%, indicating the maximum number of concurrent tags is no more than 10. The R-R interval estimation error increases with the number of users increasing.

This is because multiple tags share the inventory time slot of the reader. With the number of tags increasing, the reading rate per tag decreases, resulting in missing RSS and phase samples. To cope with this problem, we employ an interpolation method to interpolate missing samples to increase the sensing accuracy. That's why the system maintains an accuracy of over 88.8% when the number of users increases to 10. The results imply that ZeroEcg is capable of concurrently sensing 10 users' ECG signals.

5.4 Impact of Various Factors

Impact of the environmental noise. To create a dynamic environment, we ask 1, 2, 3, and 4 volunteers to walk around a user equipped with a ZeroEcg tag. The distance between volunteers and the ZeroEcg tag is about 30 cm. From Fig. 18, we observe that the QRS detection accuracy is higher than 94.8%, and the median R-R interval error is small, i.e., less than 0.08 s. These results demonstrate that the ZeroEcg is robust to the environment noise and can be used in real-world scenarios.

Impact of the user's motion. We evaluate ZeroEcg when a user is in three motion states: static, body swinging back and forth, and walking at a speed of 3 km/h. From Fig. 19, we observe that the averaged QRS detection accuracy is higher than 92%, and the median R-R interval estimation error is less than 0.082 s. These results demonstrate that the ZeroEcg is robust to the user's motion and can be used in daily activities.

Impact of the user's cloth. In real-world applications, the user may wear different clothes when the temperature changes. This experiment evaluates the impact of cloth on the ECG sensing performance. We ask the volunteer to wear a T-shirt, sweater, down coat, and no clothes respectively. We test the ECG signal for each setting using our ZeroEcg and the ground truth ECG machine. Results in Fig. 20 show that the average sensing accuracy of these four cases is over 93.7%, and the median R-R interval error is less than 0.11 s. Moreover, we observe no correlation between the sensing performance and the cloth type, demonstrating that the cloth has no impact on the ECG sensing performance.

Robustness on different distances and relative positions. In practical applications, the relative position between the reader and the tag will change, resulting in varying distances and relative orientations. We change the distance between a ZeroEcg tag and an RFID reader from 0.2 m to 2 m at a step size of 0.2 m. From Fig. 21, we observe that the QRS detection accuracy is more than 92.9% and the median R-R interval error is lower than 0.11 s when the distance is within 1.6 m. The sensing performance slightly decreases when the distance is over 1.6 m.

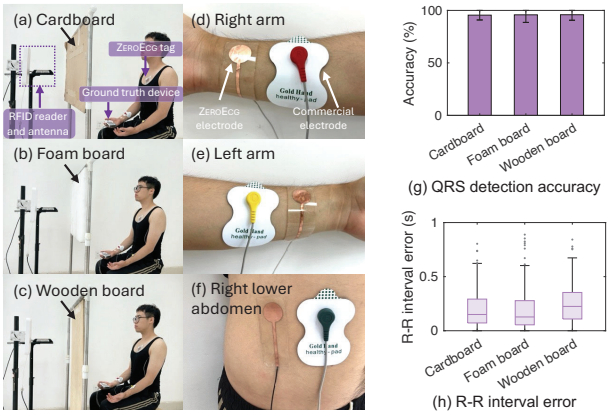

Figure 23: The NLoS scenario setups with three types of blockage objects (a-c), the synchronized electrode connections (d-f), and ECG sensing results (g, h).

Then, we test the ECG sensing performance on different relative positions as shown in Fig. 22(a). Results in Fig. 22(b) show that the QRS detection accuracy decreases slightly with the relative distance increase, while the accuracy is still higher than 90%. Also, the R-R interval error gets higher as the tag gets farther from the reader and the tag-reader's relative angle gets larger. This is because the reader's antenna radiation gain gradually decreases as the radiation angle gets larger, resulting in lower signal strength and reading rate. Overall, ZeroEcg is robust for the relative position changes as long as the tag is placed within the effective radiation region of the reader antenna.

Performance in NLoS scenarios. In this experiment, we investigate the sensing performance in non-line-of-sight (NLoS) scenarios, where the direct line-of-sight path between the reader and the tag is obstructed by objects as shown in Fig. 23 (a)-(c). We test the impact of three blockage objects, i.e., the cardboard, the foam board, and the wooden board respectively. The distance between the reader antenna and the ZeroEcg tag is 40 cm. Furthermore, since the ground truth device needs three separate electrode connections, we connect the ECG electrodes to the PCB circuit's three pins via conduct lines. To make sure that the measured ECG wave of ZeroEcg tag is the same as the ground truth ECG wave, we stick the three electrodes of ZeroEcg tag at the same position as the ground truth electrodes, i.e., the right arm (RA), the left arm (LA), and the right lower abdomen (RL) [7] as shown in Fig. 23 (d)-(f). The commercial electrodes are connected to the ground truth ECG device. Fig. 23 (g) and (h) show the results. The mean QRS detection accuracy is higher than 95% in all three NLoS scenarios. Under the three blockage conditions, the median R-R interval errors are 0.15 s, 0.12 s, and 0.22 s, increased by 0.08 s, 0.05 s, and 0.14 s, compared to the LoS scenario. Results demonstrate that the ECG sensing performance slightly decreases in NLoS scenarios due to the signal attenuation and decreased reading rate.

[7] Note that placing the reference electrode on the right lower abdomen or the right leg will measure the same ECG wave. Here, we put the reference electrode on the right lower abdomen for the sake of convenience.

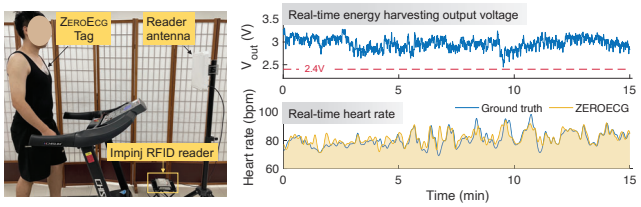

(a) Experimental setup (b) Real-time results over 15 minutes

Figure 24: Battery-free and continuous ECG sensing.

5.5 Case Study: Battery-Free ECG Sensing

We validate the effectiveness of ZeroEcg in continuous ECG sensing with real-time RF energy harvesting. Specifically, we ask a user attached with a ZeroEcg tag to walk on a treadmill at a speed of 3 km/h. The reader antenna is placed in front of the treadmill and around half a meter away from the ZeroEcg tag, as shown in Fig. 24(a). The measured output voltage of the RF energy harvesting circuit over 15 minutes is shown in the upper subfigure in Fig. 24(b). The output voltage is always higher than the required minimum input voltage of LDO (i.e., 2.4 V), indicating that the designed energy harvesting circuit can continuously drive our ZeroEcg tag. It is also noted that the voltage fluctuates since the user's movement while walking changes the reader-tag distance slightly. The bottom subfigure in Fig. 24(b) shows the ground truth heart rate and ZeroEcg estimated heart rate over 15 minutes. The estimation is very close to the ground truth. In summary, these results show the effectiveness of ZeroEcg in battery-free and continuous ECG sensing.

6 RELATED WORK

Commercial ECG monitoring devices. Existing commercial dedicated ECG devices can be divided into three categories: (i) professional medical ECG equipment, (ii) miniaturized portable devices, and (iii) smartwatches. Although professional medical equipment is accurate [22], it is expensive and requires patients to lie on a bed with many cable connections, which limits its usability and user activities. The portable ECG device [35, 38, 39] is easy to use and can be self-monitored by users. However, it requires recharging batteries frequently, preventing continuous ECG monitoring. In addition, smartwatches have been developed with ECG measurement function [21, 31]. However, the smartwatch requires the user to keep two hands in contact with the dial to realize instant ECG measurement, which is inconvenient for continuous ECG monitoring during activities. Unlike commodity ECG devices, the ZeroEcg tag has three

advantages: (*i*) it does not need complex cable connections, making it convenient for daily use without interfering with the user's activities; (*ii*) it enables continuous ECG monitoring; (*iii*) it is significantly more affordable than traditional wearable devices. The disadvantage of the ZeroEcg tag is the resolution of the recovered ECG waveform is limited by the reader's low reading rate, resulting in lower accuracy than the commodity ECG devices.

RF-based contactless heart-related signal sensing. The contactless sensing approach obviates the need for users to wear any devices, thereby affording user comfort. Several works exploit RFID or mmWave signals to sense the heartbeat or heart's vibrations, i.e., Seismocardiography (SCG). For example, studies [65, 71] propose attaching RFID tags to the chest to detect the heart micro-vibration. Further, works [48, 70] use mmWave reflection signals from the chest to monitor the heart SCG signal. Recently, Xu *et al.* [44] utilize deep learning to map the SCG signal to the ECG signal. Unlike these works, ZeroEcg measures the heart electric signal ECG obtained from stick-on ECG electrodes.

Low-power RFID sensing. Various RFID sensing systems have been proposed for low-power sensing applications, which can be roughly divided into two categories. One is to leverage the changes in the RFID tag's antenna impedance or the changes in the RFID tag's backscattered channel caused by targets [51, 57, 60, 66, 67, 69]. However, ECG signals cannot change these two physical features of RFID tags, making this sensing principle fail in ECG sensing. The other approach is to integrate the sensor with a COTS RFID chip (e.g., SL900A [20] and Farsen Rocky100 [4]) or customized RFID sensor platform (e.g., WISP [63] and GoodID [52]). However, the limited power harvesting ability of the sensory RFID chip-based tag cannot provide a continuous power supply for an external MCU and data conversion and storage [4]. GoodID [52] embeds the SPI sensor's output signal into the tag's EPC reply directly and thus eliminates the high-power MCU for data storage, which however requires SPI-compatible sensors. Besides, Besnoff *et al.* [43] design a digital ECG biotelemetry chip to sense the ECG signal and a backscatter circuit to transmit the ECG signal to a remote reader. However, this system requires MCU, ADC, and DAC components and consumes 1.23 mW, which is challenging in realizing continuous and battery-free ECG sensing. Differing from the above solutions, ZeroEcg modulates the sensor's analog signal on the RFID tag's RSS and phase feature, which eliminates the power consumption of data conversion and storage and can adapt to general sensors.

7 DISCUSSION AND FUTURE WORKS

Expanding application scenarios. So far, the application scenario of ZeroEcg is limited to specific regions where an RFID reader is deployed such as a hospital room, a bedroom, or a living room, and a treadmill in gyms. The key limitation remains in harvesting sufficient power for continuously powering the ZeroEcg tag. To overcome this challenge, one feasible solution is to realize beamforming with multiple readers [46, 54] to improve the reader-tag distance. The other is to employ hand-holding mobile readers. We noticed that there is a commercial hand-holding mobile RFID reader such as Chainway C66 [41], which provides the possibility of spanning the full range of physical spaces in daily life.

Low sensing accuracy and scaling limit. The current ECG sensing results show lower sensing accuracy than the commodity ECG monitoring devices and low concurrency. This is because the RFID reader's reading rate limits the ECG sensing accuracy and the system scaling limit. A possible signal processing solution is to exploit a deep learning-based method to reconstruct high-resolution ECG waveforms [48]. In this way, one can improve the ECG sensing accuracy and increase the number of concurrent sensing users. In future work, we will exploit recent advanced deep-learning methods to realize high-accuracy ECG signal reconstruction and abnormal feature identification.

8 CONCLUSION

This paper presents ZeroEcg, a wireless, battery-free, lightweight, electronic-skin-like tag for ECG sensing, without disturbing human activities. By exploring and leveraging the RFID MOSFET switch, we modulate ECG signals to the RFID received signal strength (RSS) and phase feature. Furthermore, by designing a passive interference removal circuit and optimized energy harvesting circuit, ZeroEcg tag can continuously capture and transmit the weak ECG signal in a battery-free manner. Extensive experiments demonstrate the effectiveness of ZeroEcg in various real-world settings.

ACKNOWLEDGMENTS

This work is supported by NSFC under Grant (62372372, 62172332), NSFC A3 under Grant 62061146001, Shaanxi Science and Technology Innovation Team Program under Grant 2024RSCXTD05, and Shaanxi International Science and Technology Cooperation Program under Grant 2024GH-YBXM-07. We thank our shepherd and anonymous reviewers for their valuable feedback. We thank Prof. Xinliang Zheng, Prof. Guangyin Jing, and Dr. Hao Luo for their helpful discussions. We thank Prof. Srinivasan Keshav and Omid Abari for their valuable feedback. We thank participants who voluntarily participated in the experiments described in this paper.

REFERENCES

[1] Impinj speedway r420 rfid reader, 2012-2023. https://www.impinj.com/products/readers/impinj-speedway.

[2] Epc-gen2 protocol, 2015. https://www.gs1.org/sites/default/files/docs/epc/Gen2_Protocol_Standard.pdf.

[3] Sudden cardiac arrest during sports activity in middle age, 2015. https://www.acc.org/latest-in-cardiology/articles/2015/09/29/11/34/sudden-cardiac-arrest-during-sports-activity-in-middle-age.

[4] Epc c1g2 compliant uhf rfid tag with power harvesting and spi communication for external low power sensors and actuators, 2018. http://www.rtutech.com/28web/Upload/20181225105747967.pdf.

[5] Frequency response of thin film chip resistors, 2018. https://www.vishay.com/docs/53077/microwavethinfilmres.pdf.

[6] Microwave thin film resistors - ch series, 2018. https://www.vishay.com/docs/53077/microwavethinfilmres.pdf.

[7] Usa: Amazon warehouse worker who died of heart attack at work reportedly left on the floor for 20 minutes before receiving treatment, 2019. https://www.business-humanrights.org/en/latest-news/usa-amazon-warehouse-worker-who-died-of-heart-attack-at-work-reportedly-left-on-the-floor-for-20-minutes-before-receiving-treatment/.

[8] 5 dbi rubber duck antenna 900-930mhz, 2020. https://www.pasternack.com/single-antenna-900-930-mhz-5-dbi-gain-sma-pe51rd1010-p.aspx.

[9] Auto parts worker dies of covid-19-induced heart attack at faurecia plant in saline, michigan, 2020. https://www.wsws.org/en/articles/2020/12/10/sal2-d10.html.

[10] Circular polarity rfid panel antenna, 2021. https://www.lairdconnect.com/documentation/ant-ds-s9028pcl-s9028pcr-0515pdf.

[11] 5 reasons to implement rfid wristbands for gym, 2022. https://www.asiarfid.com/rfid-wristbands-for-gym.html.

[12] Easy ecg monitor – prince 180b1, 2022. http://www.healforce.com/en/html/products/portableecgmonitors/605.html.

[13] Nxp g2il chip, 2022. https://www.nxp.com/docs/en/data-sheet/SL3S1203_1213.pdf.

[14] Rfid chemistry, 2022. https://www.dipolerfid.com/rfid-chemistry.

[15] 12-lead holter monitor, 2023. https://getwellue.com/products/12-lead-holter-monitor.

[16] 24-hour ecg recorder, 2023. https://getwellue.com/products/heart-health-monitor.

[17] Ad8232, 2023. https://www.analog.com/en/products/ad8232.html#product-overview.

[18] Aln-9662, 2023. https://www.alientechnology.com/wp-content/uploads/Alien-Technology-Higgs-3-ALN-9662-Short.pdf.

[19] Aln-9740, 2023. https://www.alientechnology.com/wp-content/uploads/Alien-Technology-Higgs-4-ALN-9740-Squiggle.pdf.

[20] Ams sl900a rfid tag chip, 2023. https://ams.com/zh/sl900a.

[21] Apple watch series 8, 2023. https://www.apple.com/sg/apple-watch-series-8/.

[22] Biocare digital electrocardiograph high-end 12-channel ecg machine, 2023. https://getwellue.com/products/biocare-12-lead-12-channel-ecg-machine.

[23] Cement factory worker dies of heart attack, triggers stir: Police, 2023. https://www.devdiscourse.com/article/politics/1405843-cement-factory-worker-dies-of-heart-attack-triggers-stir-police.

[24] The ecg leads: Electrodes, limb leads, chest(precordial) leads and the 12-lead ecg, 2023. https://ecgwaves.com/topic/ekg-ecg-leads-electrodes-systems-limb-chest-precordial/.

[25] Ecoflex 00-30, 2023. https://www.smooth-on.com/products/ecoflex-00-30/.

[26] Ekg machines | ecg machines, 2023. https://www.becklee.com/ekg-machines.html.

[27] Electrocardiogram (ecg/ekg), 2023. https://www.heartandstroke.ca/heart-disease/tests/electrocardiogram#:~:text=An%20electrocardiogram%20(ECG%20or%20EKG,pump%20blood%20from%20the%20heart.

[28] How rfid improves gym management, 2023. https://www.rfidcard.com/how-rfid-improves-gym-management/.

[29] How to modulate on uhf-rfid tag?, 2023. http://amplet.tokyo/rfid/r_page04eng.html.

[30] Hsms-285c, 2023. https://www.alldatasheet.com/datasheet-pdf/pdf/935820/BOARDCOM/HSMS-285C.html.

[31] Huawei watch series 4, 2023. https://consumer.huawei.com/cn/wearables/watch-4-series/.

[32] Man dies of heart attack while running on treadmill at ghaziabad gym, 2023. https://www.ndtv.com/india-news/man-dies-of-heart-attack-while-running-on-treadmill-at-ghaziabad-gym-4396059.

[33] Man suffers cardiac arrest while driving and crashes car | ambulance, 2023. https://www.youtube.com/watch?v=pXZ_zdnnu64.

[34] Nasiff pc-based excercise stress test system, 2023. https://www.becklee.com/nasiff-cardiostress-pc-based-system-treadmill.html.

[35] Personal ecg monitor, 2023. https://getwellue.com/pages/pulsebit-ex-ekg-monitor.

[36] Qrs interval, 2023. https://litfl.com/qrs-interval-ecg-library/.

[37] Tps7a02, 2023. https://www.ti.com/product/TPS7A02.

[38] Wellue 12-lead pocket ecg machine, 2023. https://getwellue.com/products/12-lead-pocket-ecg-machine.

[39] Wellue ecg recorder, 2023. https://getwellue.com/products/heart-health-monitor.

[40] Worker at washington nissan factory dies from 'suspected heart attack', 2023. https://www.thenorthernecho.co.uk/news/23462148.worker-washington-nissan-factory-dies-suspected-heart-attack/.

[41] 2024. https://www.chainway.net/Products/Info/58.

[42] Barnett, R. E., Liu, J., and Lazar, S. A rf to dc voltage conversion model for multi-stage rectifiers in uhf rfid transponders. *IEEE Journal of solid-state circuits 44*, 2 (2009), 354–370.

[43] Besnoff, J. S., Deyle, T., Harrison, R. R., and Reynolds, M. S. Battery-free multichannel digital ecg biotelemetry using uhf rfid techniques. In *2013 IEEE international conference on RFID (RFID)* (2013), IEEE, pp. 16–22.

[44] Chen, J., Zhang, D., Wu, Z., Zhou, F., Sun, Q., and Chen, Y. Contactless electrocardiogram monitoring with millimeter wave radar. *IEEE Transactions on Mobile Computing* (2022).

[45] Colin, E., Moretto, A., Ripoll, C., and Abou Chakra, S. Delta rcs of uhf rfid taking into account the shunt resistance in the tag model. In *2009 Joint IEEE North-East Workshop on Circuits and Systems and TAISA Conference* (2009), IEEE, pp. 1–4.

[46] Fan, X., Shangguan, L., Howard, R., Zhang, Y., Peng, Y., Xiong, J., Ma, Y., and Li, X.-Y. Towards flexible wireless charging for medical implants using distributed antenna system. In *Proceedings of the 26th annual international conference on mobile computing and networking* (2020), pp. 1–15.

[47] Gu, X., de Almeida, J. V., Hemour, S., Khazaka, R., and Wu, K. Temperature-stable low-power rf-to-dc dickson charge pump rectifiers for battery-free sensing and iot systems. *IEEE Journal of Radio Frequency Identification* (2024).

[48] Ha, U., Assana, S., and Adib, F. Contactless seismocardiography via deep learning radars. In *Proceedings of the 26th annual international conference on mobile computing and networking* (2020), pp. 1–14.

[49] Ibanez, B., James, S., Agewall, S., and et al. 2017 ESC Guidelines for the management of acute myocardial infarction in patients presenting with ST-segment elevation: The Task Force for the management of acute myocardial infarction in patients presenting with ST-segment elevation of the European Society of Cardiology (ESC). *European Heart Journal 39*, 2 (08 2017), 119–177.

[50] Kashani, A., and Barold, S. S. Significance of qrs complex duration in patients with heart failure. *Journal of the American College of Cardiology 46*, 12 (2005), 2183–2192.

[51] Li, L., Xie, Y., Xiong, J., Hou, Z., Zhang, Y., We, Q., Wang, F., Fang, D., and Chen, X. Smartlens: sensing eye activities using zero-power contact lens. In *Proceedings of the 28th Annual International Conference on Mobile Computing And Networking* (2022), pp. 473–486.

[52] Li, S., Meng, Q., Bai, Y., Zhang, C., Song, Y., Li, S., and Lu, L. Go beyond rfid: Rethinking the design of rfid sensor tags for versatile applications. In *Proceedings of the 29th Annual International Conference on Mobile Computing and Networking* (2023), pp. 1–16.

[53] Liu, W., Huang, K., Wang, T., Hou, J., and Zhang, Z. A compact ultra-broadband rf rectifier using dickson charge pump. *IEEE Microwave and Wireless Components Letters 32*, 6 (2022), 591–594.

[54] Ma, Y., Luo, Z., Steiger, C., Traverso, G., and Adib, F. Enabling deep-tissue networking for miniature medical devices. In *Proceedings of the 2018 Conference of the ACM Special Interest Group on Data Communication* (2018), pp. 417–431.

[55] Mortara, J. L. *ECG Acquisition and Signal Processing*. Humana Press, 2005, pp. 131–145.

[56] Nikitin, P. V., Martinez, R., Ramamurthy, S., Leland, H., Spiess, G., and Rao, K. Phase based spatial identification of uhf rfid tags. In *2010 IEEE International Conference on RFID (IEEE RFID 2010)* (2010), IEEE, pp. 102–109.

[57] Occhiuzzi, C., Rida, A., Marrocco, G., and Tentzeris, M. Rfid passive gas sensor integrating carbon nanotubes. *IEEE Transactions on Microwave Theory and Techniques 59*, 10 (2011), 2674–2684.

[58] Pérez-Villacastín, J. Sudden cardiac death during sports practice. is one man's meat another man's poison? *Revista espanola de cardiologia (English ed.) 74*, 3 (2021), 210–212.

[59] Ponikowski, P., Voors, A. A., Anker, S. D., and et al. 2016 ESC Guidelines for the diagnosis and treatment of acute and chronic heart failure: The Task Force for the diagnosis and treatment of acute and chronic heart failure of the European Society of Cardiology (ESC)Developed with the special contribution of the Heart Failure Association (HFA) of the ESC. *European Heart Journal 37*, 27 (05 2016), 2129–2200.

[60] Pradhan, S., Chai, E., Sundaresan, K., Qiu, L., Khojastepour, M. A., and Rangarajan, S. Rio: A pervasive rfid-based touch gesture interface. In *Proceedings of the 23rd Annual International Conference on Mobile Computing and Networking* (2017), pp. 261–274.

[61] Saritha, C., Sukanya, V., and Murthy, Y. N. Ecg signal analysis using wavelet transforms. *Bulg. J. Phys 35*, 1 (2008), 68–77.

[62] Siu, C. *Diode and BJT Equations*. Springer International Publishing, 2022, pp. 205–229.

[63] Smith, J. R., Sample, A. P., Powledge, P. S., Roy, S., and Mamishev, A. A wirelessly-powered platform for sensing and computation. In *International Conference on Ubiquitous Computing* (2006), Springer, pp. 495–506.

[64] Sze, S. M., Li, Y., and Ng, K. K. *Physics of semiconductor devices*. John wiley & sons, 2021.

[65] Wang, C., Xie, L., Wang, W., Chen, Y., Bu, Y., and Lu, S. Rf-ecg: Heart rate variability assessment based on cots rfid tag array. *Proceedings of the ACM on Interactive, Mobile, Wearable and Ubiquitous Technologies 2*, 2 (2018), 1–26.

[66] Wang, J., Abari, O., and Keshav, S. Challenge: Rfid hacking for fun and profit. In *MobiCom'18* (2018), pp. 461–470.

[67] Wang, J., Chang, L., Aggarwal, S., Abari, O., and Keshav, S. Soil moisture sensing with commodity rfid systems. In *Proceedings of the 18th International Conference on Mobile Systems, Applications, and Services* (2020), pp. 273–285.

[68] Wang, J., Li, J., Mazaheri, M. H., Katsuragawa, K., Vogel, D., and Abari, O. Sensing finger input using an rfid transmission line. In *Proceedings of the 18th Conference on Embedded Networked Sensor Systems* (2020), pp. 531–543.

[69] Wang, J., Xiong, J., Chen, X., Jiang, H., Balan, R. K., and Fang, D. Tagscan: Simultaneous target imaging and material identification with commodity rfid devices. In *Proceedings of the 23rd Annual International Conference on Mobile Computing and Networking* (2017), pp. 288–300.

[70] Xu, C., Li, H., Li, Z., Zhang, H., Rathore, A. S., Chen, X., Wang, K., Huang, M.-c., and Xu, W. Cardiacwave: A mmwave-based scheme of non-contact and high-definition heart activity computing. *Proceedings of the ACM on Interactive, Mobile, Wearable and Ubiquitous Technologies 5*, 3 (2021), 1–26.

[71] Zhao, R., Wang, D., Zhang, Q., Chen, H., and Huang, A. Crh: A contactless respiration and heartbeat monitoring system with cots rfid tags. In *2018 15th annual IEEE international conference on sensing, communication, and networking (SECON)* (2018), IEEE, pp. 1–9.